AGU PUBLICATIONS

JGR

Journal of Geophysical Research: Atmospheres

RESEARCH ARTICLE
10.1002/2017JD027002

Key Points:
- Tropical mean daytime and nighttime OLR show consistent decreasing trends between 2003 and 2013 from different data sets due to ENSO events
- All data sets show that the daytime OLR decreases faster than that of the nighttime during this time period
- Cloud properties from different sensors are examined to understand the cause of the faster decreasing daytime trend than nighttime trend

Correspondence to:
W. Su,
wenying.su-1@nasa.gov

Citation:
Su, W., N. G. Loeb, L. Liang, N. Liu, and C. Liu (2017), The El Niño-Southern Oscillation effect on tropical outgoing longwave radiation: A daytime versus nighttime perspective, *J. Geophys. Res. Atmos.*, *122*, 7820–7833, doi:10.1002/2017JD027002.

Received 20 APR 2017
Accepted 11 JUL 2017
Accepted article online 20 JUL 2017
Published online 5 AUG 2017

The El Niño–Southern Oscillation effect on tropical outgoing longwave radiation: A daytime versus nighttime perspective

Wenying Su[1], Norman G. Loeb[1], Lusheng Liang[2], Nana Liu[3], and Chuntao Liu[3]

[1]NASA Langley Research Center, Hampton, Virginia, USA, [2]Science Systems and Applications, Inc., Hampton, Virginia, USA, [3]Department of Physical and Environmental Sciences, Texas A&M University-Corpus Christi, Corpus Christi, Texas, USA

Abstract Trends of tropical (30°N–30°S) mean daytime and nighttime outgoing longwave radiations (OLRs) from the Clouds and Earth's Radiant Energy System (CERES) and the Atmospheric Infrared Sounder (AIRS) are analyzed using data from 2003 to 2013. Both the daytime and nighttime OLRs from these instruments show decreasing trends because of El Niño conditions early in the period and La Niña conditions at the end. However, the daytime and nighttime OLRs decrease at different rates with the OLR decreasing faster during daytime than nighttime. The daytime-nighttime OLR trend is consistent across CERES Terra, Aqua observations, and computed OLR based upon AIRS and Moderate-Resolution Imaging Spectroradiometer (MODIS) retrievals. To understand the cause of the differing decreasing rates of daytime and nighttime OLRs, high cloud fraction and effective temperature are examined using cloud retrievals from MODIS and AIRS. Unlike the very consistent OLR trends between CERES and AIRS, the trends in cloud properties are not as consistent, which are likely due to the different cloud retrieval methods used. When MODIS and AIRS cloud properties are used to compute OLR, the daytime and nighttime OLR trends based upon MODIS cloud properties are approximately half as large as the trends from AIRS cloud properties, but their daytime-nighttime OLR trends are in agreement. This demonstrates that though the current cloud retrieval algorithms lack the accuracy to pinpoint the changes of daytime and nighttime clouds in the tropics, they do provide a radiatively consistent view for daytime and nighttime OLR changes. The causes for the larger decreasing daytime OLR trend than that for nighttime OLR are not clear and further studies are needed.

Plain Language Summary In this study, trends of tropical (30°N–30°S) mean daytime and nighttime outgoing longwave radiations (OLRs) from the Clouds and Earth's Radiant Energy System (CERES) and the Atmospheric Infrared Sounder (AIRS) instruments are analyzed using data from January 2003 to December 2013. Both the daytime and the nighttime OLR data records from these instruments show decreasing trends owing to the occurrence of El Niño conditions early in the period and La Niña conditions at the end. However, the daytime and nighttime OLRs decrease at different rates with the daytime OLR decreasing faster than the nighttime OLR. The daytime-nighttime OLR trend is consistent across CERES Terra, Aqua observations, and computed OLR based upon AIRS and MODIS retrievals. Cloud retrievals from multiple satellite sensors are examined to understand the cause of the changes in OLR.

1. Introduction

The top-of-the-atmosphere outgoing longwave radiation (OLR) is an important component of the Earth's radiation energy budget and has been monitored globally from space since the 1970s. Currently, both the Clouds and Earth's Radiant Energy System (CERES) and the Atmospheric Infrared Sounder (AIRS) provide the global OLR data products. Knowledge of decadal and interannual variations of OLR is important for understanding changes in the Earth's radiation energy balance [*Loeb et al.*, 2009; *Trenberth et al.*, 2009; *Loeb et al.*, 2016]. Changes in sea surface temperature (SST) and in cloud properties are often reflected in changes in OLR, thus OLR (or longwave cloud radiative effect) is often used in diagnosing tropical interannual variability [*Wong et al.*, 2006; *Loeb et al.*, 2012; *Zelinka and Hartmann*, 2011; *Wang and Su*, 2015]. *Zelinka and Hartmann* [2011] found that during El Niño the tropical mean high cloud cover decreases (which raises OLR), while the height of these clouds increases (which lowers OLR). The high cloud cover changes tend to dominate over changes in cloud height, so that tropical mean OLR increases during El Niño period.

Satellite data sets were also instrumental for understanding the diurnal cycles of OLR over different surface types [i.e., *Hartmann and Recker*, 1986; *Harrison et al.*, 1988; *Gruber and Chen*, 1988]. *Hartmann and Recker* [1986] found large OLR diurnal variations over most land areas with the maximum OLR near noon, while the diurnal variations in OLR are generally less than 5 Wm^{-2} over oceanic stratus with the maximum occurring between mid-to-late afternoon. They also found that over convective ocean regions, the diurnal cycle of OLR is strongly modulated by the diurnal cycle of clouds. *Taylor* [2012] investigated the diurnal cycle of OLR using the CERES synoptic (SYN) [*Doelling et al.*, 2013] product and concluded that the diurnal cycles of OLR over land and ocean are consistent with the previous studies, except that the amplitude derived using CERES data is larger than indicated previously.

In the tropical region where high clouds are prevalent, the diurnal variations of OLR are strongly related to that of high clouds. Over land the maximum deep convection and precipitation occur in the afternoon, while over ocean the maximum occurs in the early morning [*Yang and Slingo*, 2001; *Tian et al.*, 2004]. The diurnal variations of deep convection and precipitation are relatively weaker over ocean than over land [*Chen and Houze*, 1997; *Sui et al.*, 1998; *Tian et al.*, 2004; *Liu and Zipser*, 2008]. The reasons why oceanic convective clouds exhibit a diurnal cycle are unclear. *Gray and Jacobson* [1977] proposed that the atmosphere surrounding organized cloudy regions adjust to large-scale radiative cooling at night through extra subsidence, which increases low-level convergence into the adjacent cloudy regions. During daytime, solar heating reduces tropospheric radiation loss, and the clear region subsidence warming and low-level convergence are substantially weakened. The mechanism developed by *Randall et al.* [1991] and *Xu and Randall* [1995] focused on direct radiation-convection interactions. At night, longwave cooling at cloud top destabilizes the upper troposphere, thereby invigorating convective development with a maximum in the early morning. During daytime, clouds absorb solar radiation and stabilize the atmosphere and suppress the convection. *Chen and Houze* [1997] argued that cloud-radiation interactions can only partially explain the diurnal variability of deep convection over tropical oceans and stressed the need to take both the life cycle of the cloud systems and the diurnal solar heating of the ocean surface and atmospheric boundary layer into account in order to understand the diurnal variability.

El Niño–Southern Oscillation (ENSO) is the dominant mode of natural interannual climate variability in the tropics. Many studies have focused on how different ENSO events affect the clouds and OLR in the tropics [*Zelinka and Hartmann*, 2011; *Loeb et al.*, 2012; *Su and Jiang*, 2013; *Wang and Su*, 2015]. All these studies used diurnally averaged OLR and/or cloud radiative effects. As the tropical convective clouds have distinct diurnal cycles over ocean and land, it is important to understand whether the SST changes associated with ENSO events would affect the daytime and nighttime clouds differently. In this study, we used AIRS Version 6 and CERES Edition 4 Terra and Aqua OLR from January 2003 to December 2013 to investigate how daytime and nighttime OLRs respond to SST changes during this time period. Both daytime and nighttime OLR records from CERES and AIRS show consistent decreasing trends, with the daytime trends greater than nighttime resulting in statistically significant decreasing trends in day-night OLR trends. High cloud fractions and effective temperatures from Moderate-Resolution Imaging Spectroradiometer (MODIS) and AIRS retrievals are examined to understand the differing daytime and nighttime OLR trends.

2. Data and Analysis Method

The CERES instrument consists of a three-channel broadband scanning radiometer [*Wielicki et al.*, 1996]. The scanning radiometer measures radiances in shortwave (SW, 0.3–5 μm), window (WN, 8–12 μm), and total (0.3–200 μm) channels at a spatial resolution of ~20 km at nadir. The longwave (LW) component is derived as the difference between total and SW channels. Thus far, six CERES instruments have flown on four different satellites. In this study, CERES measurements aboard NASA's Earth Observing System (EOS) Terra and Aqua satellites are used. CERES instruments (Flight Model (FM) 1 and 2) on Terra were launched on 18 December 1999, into a 705 km Sun-synchronous orbit with a 10:30 A.M. equatorial crossing time. CERES instruments (FM3 and FM4) on Aqua were launched on 4 May 2002, into a 705 km Sun-synchronous orbit with a 1:30 P.M. equatorial crossing time. CERES on Terra and Aqua flies alongside Moderate-Resolution Imaging Spectroradiometer (MODIS). The high-resolution MODIS imager provides cloud conditions for every CERES footprint. The CERES/MODIS cloud algorithms retrieve cloud fraction (f, in percent), cloud optical depth, cloud phase, cloud top, and effective temperature/pressure (among other variables) based on MODIS pixel level measurements [*Minnis et al.*, 2010]. These pixel level cloud properties are spatially and temporally matched with the CERES footprint and are used to select the scene-dependent angular distribution models to convert the CERES measured radiances to fluxes [*Su et al.*, 2015].

Table 1. List of Satellite Instruments and Their Retrieved Products Used in This Paper[a]

Satellite	Instrument	Products
Terra	CERES	observed OLR/WN flux, and calculated OLR
Aqua	CERES	observed OLR/WN flux, and calculated OLR
Aqua	AIRS	calculated OLR, f, T_{eff}
Terra	MODIS	f, T_{eff}
Aqua	MODIS	f, T_{eff}
TRMM	VIRS	Tb11
CALIPSO	CALIOP	$f(z)$

[a]OLR is the TOA outgoing longwave radiation, WN is the TOA window (8–12 μm) flux, f is cloud fraction, T_{eff} is the cloud effective temperature, Tb11 is the VIRS 10.8 μm brightness temperature, and $f(z)$ is the cloud fraction vertical distribution derived from CALIPSO lidar. TRMM, Tropical Rainfall Measuring Mission; CALIOP, Cloud-Aerosol Lidar with Orthogonal Polarization; VIRS, Visible and Infrared Sensor; and CALIPSO, Cloud-Aerosol Lidar and Infrared Pathfinder Satellite Observation.

The CERES Edition 4 Single Scanner Footprint top of the atmosphere (TOA)/Surface Fluxes and Clouds (SSF) product from January 2003 to December 2013 is used in this study. SSF product contains the instantaneous SW and LW fluxes, and the cloud properties derived using the MODIS (for Terra and Aqua) spectral channels. Daytime and nighttime instantaneous TOA fluxes are averaged into monthly 1° latitude by 1° longitude gridded product. Daytime and nighttime cloud properties within each 1°×1° grid box are weighted by cloud fraction to provide the respective grid box mean values.

The CERES synoptic radiative fluxes and clouds product provide cloud properties and calculated flux profiles for each 1° latitude by 1° longitude (SYN1deg, [*Doelling et al.*, 2013]). SW and LW fluxes at surface, 500 hPa, 200 hPa, 70 hPa, and TOA are calculated using a fast radiative transfer model developed by *Fu and Liou* [1993] and subsequently modified by the CERES team [*Rose et al.*, 2013]. Cloud properties retrieved from the MODIS observations, aerosol properties from MODIS and an aerosol transport model (MATCH) [*Collins et al.*, 2001], and temperature/humidity profiles from Goddard Modeling and Assimilation Office's (GMAO) reanalysis version 5.4.1 are used as inputs to the radiative transfer calculation (see details in *Rose et al.* [2013]). Edition 4 SYN1deg data are used in this study. The CERES and MODIS data products (along with all other data products from instruments discussed in this section) used in this analysis are summarized in Table 1.

The Atmospheric Infrared Sounder (AIRS) instrument is also on the Aqua satellite and is a thermal infrared grating spectrometer operating along side the Advanced Microwave Sounding Unit (AMSU). AIRS has 2378 spectral channels that cover the spectrum from 3.7 to 15.4 μm and with a nadir footprint size of 13.5 km. AIRS/AMSU employs cloud clearing technique [*Susskind et al.*, 2003] to infer the clear-sky radiance over the entire AIRS spectral range. The cloud-cleared AIRS radiances are used to retrieve vertical profiles of temperature, water vapor, ozone, and other trace gases, along with atmospheric and surface properties. The cloud top temperature and effective cloud fraction for up to two layers are derived by comparing the AIRS observed radiances to calculated radiances using AIRS retrieved surface and atmospheric properties [*Kahn et al.*, 2014]. These AIRS/AMSU sounding products and cloud properties are then used as inputs to a radiative transfer algorithm to compute the OLR [*Susskind et al.*, 2011]. We use the AIRS Version 6 Level 3 monthly 1° latitude by 1° longitude gridded products [*Tian et al.*, 2013], which are separated into ascending (daytime) and descending (nighttime) portion of the orbit. The Level 3 data also contain coarse cloud layer products which provide cloud properties averaged over three cloud layers with the layer boundaries at surface, 680 hPa, 440 hPa, and 10 hPa. However, the AIRS cloud properties were averaged without using cloud fraction weighting (B. Tian, personal communication, 2017).

The Cloud-Aerosol Lidar and Infrared Pathfinder Satellite Observation (CALIPSO) was launched on 28 April 2006 and flies in formation with the Aqua satellite. CALIPSO Level 2 cloud layer and cloud profile data of 5 km horizontal resolution (CAL_LID_L2_05kmCLay-Standard-v4-10 and CAL_LID_L2_05kmCPro-Standard-v4-10) are used to investigate how cloud vertical distribution changes during El Niño and La Niña over the tropical region. The CLay product has a vertical resolution of 30 m from the surface to 8.2 km and 60 m from 8.2 km to 20.2 km, and the detailed algorithm description is provided in *Vaughan et al.* [2009]. The CPro product

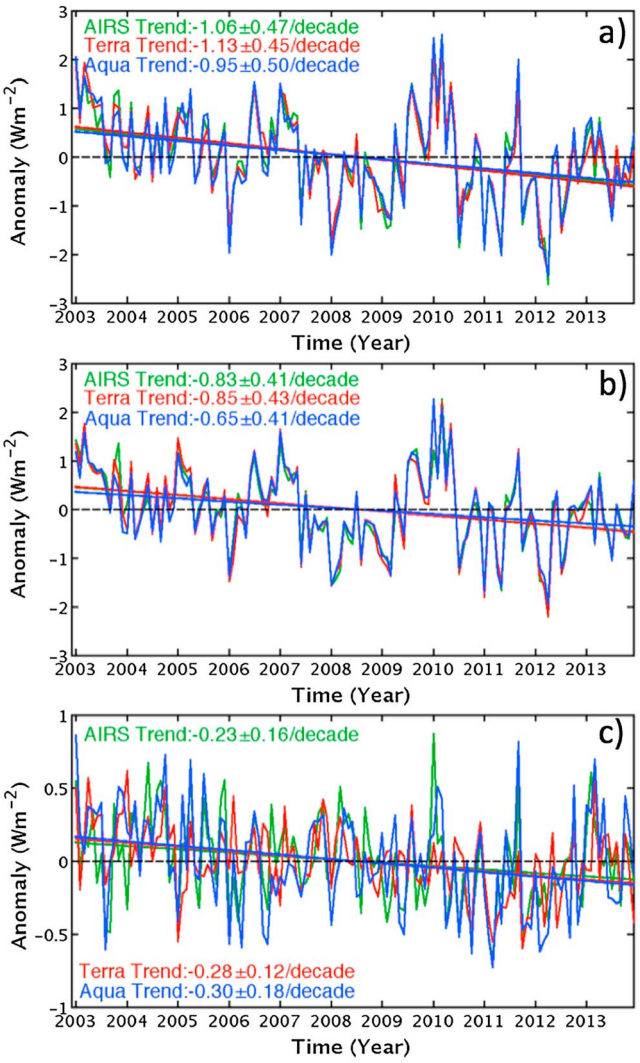

Figure 1. Deseasonalized tropical (30°N–30°S) outgoing longwave radiation (OLR, in Wm^{-2}) anomalies and trends ($Wm^{-2}Decade^{-1}$) derived from AIRS, CERES Terra, and CERES Aqua based upon (a) daytime measurements, (b) nighttime measurements, and (c) the daytime minus nighttime measurements.

has a uniform vertical resolution of 60 m. CALIPSO cloud layers are identified using different horizontal averaging (5 km, 20 km, or 80 km), which can result in a single cloud layer being reported as multiple overlapping vertical layers. For CLay product, we define a footprint as cloudy if its cloud optical depth is greater than 0.3, which is vertically integrated from the top layer to the bottom layer. We chose this value to circumvent the CALIPSO detection efficiency differences between daytime and nighttime measurements [*Thorsen et al.*, 2013] and also to be close to the passive sensors' detection limit. For each footprint, the CLay data may contain up to 10 layers of clouds. Within a grid and for a cloudy 5 km footprint, the topmost cloud layer of all vertically separated cloud layers is binned into 0.3 km altitude bins based on the topmost cloud layer height and single shot cloud-cleared fraction (the fraction of cloud free area for a cloud layer within the 5 km horizontal distance). Cloud fraction within a vertical bin is calculated as the ratio of the number of cloudy footprints to the total number of footprints. The derived cloud vertical distribution favors the highest cloud layers which are more closely linked to OLR and also minimizes the impact of different horizontal averaging. Differing from CLay product which contains the information of each isolated cloud layer, CPro data report the "Cloud Layer Fraction" which defines the cloud fraction within every 60 m vertical interval for a given 5 km footprint. Note that this cloud layer fraction was derived without applying any cloud optical depth threshold. The daytime and nighttime CLay and CPro data are gridded into 10° latitude by 10° longitude grids for each month and then averaged to provide the tropical seasonal means.

The Tropical Rainfall Measuring Mission (TRMM) was launched on 27 November 1997 into a 350 km circular, precessing orbit with a 35° inclination angle [*Kummerow et al.*, 1998]. On board the TRMM, the Visible and Infrared Sensor (VIRS) had collected the radiance at five visible and infrared channels (0.63, 1.6, 3.75, 10.8, and 12 μm) with stable calibration [*Lyu and Barnes*, 2008]. TRMM has a 46 day repeat cycle, so that a full range of solar zenith angles is acquired over a region every 46 days. VIRS brightness temperature at 10.8 μm (Tb11) is used to investigate the diurnal variations of cloud top. The total number of VIRS pixels and the numbers of pixels with Tb11 colder than 235 K and 210 K are composited into monthly local hour bins for each 2° latitude by 2° longitude grid. The occurrence frequency for cloud top colder than 235 K/210 K is calculated by dividing the number of pixels with Tb11 colder than 235 K/210 K by the total number of pixels.

3. Results

Figure 1 shows the deseasonalized anomalies of OLR derived from AIRS, CERES Terra, and CERES Aqua separately for daytime and nighttime observations over the tropics (30°S to 30°N, both land and ocean).

Table 2. Trends and 95% Confidence Intervals of OLR (Wm^{-2} $decade^{-1}$) Calculated From CERES Terra, CERES Aqua, and AIRS Retrievals, and From the CERES SYN1deg Calculated OLR[a]

	Daytime	Nighttime	Day-Night
CERES/Terra	-1.13 ± 0.45	-0.85 ± 0.43	-0.28 ± 0.12
CERES/Aqua	-0.95 ± 0.50	-0.65 ± 0.41	-0.30 ± 0.18
AIRS	-1.06 ± 0.47	-0.83 ± 0.41	-0.23 ± 0.16
SYN calculated	-0.63 ± 0.42	-0.33 ± 0.40	-0.31 ± 0.11

[a]Trends are derived using data from January 2003 to December 2013.

Both daytime and nighttime OLRs show decreasing trends. The daytime OLR trends are −1.13, −0.95, and −1.06 Wm^{-2} per decade for CERES Terra, CERES Aqua, and AIRS, and the nighttime trends are −0.85, −0.65, and −0.83 Wm^{-2} per decade, respectively. All these trends are significant at the 95% confidence level (see Table 2). The decreasing trends of daytime and nighttime OLRs are also significant when we examine the tropical land and ocean separately. The consistent variability of AIRS and CERES OLR was also noted by *Susskind et al.* [2012] using diurnally averaged CERES OLR. This decreasing trend is due to the fact that the period used in this study is dominated by El Niño events at the beginning and by La Niña events near the end. These natural ENSO variabilities resulted in a decreasing trend of the tropical mean surface temperature with distinct regional features associated with ENSO events (Figure 2).

As pointed out by *Zelinka and Hartmann* [2011], the tropical mean high cloud fraction decreases while the high cloud height increases during El Niño events, and the impact of cloud fraction on OLR dominates that of cloud height, thus resulting in an increase in OLR. The opposite occurs during the La Niña events which leads to decreased OLR. Figure 3 shows cloud fraction as a function of altitude derived from CALIPSO CPro and CLay product over the tropics during an El Niño event (December 2009 to February 2010) and a La Niña event (December 2010 to February 2011). The cloud vertical distributions derived using "cloud layer fraction" provided in CPro show large day and night difference due to detection efficiency differences between daytime and nighttime measurements [*Thorsen et al.*, 2013], but both daytime and nighttime observations show that clouds above 15 km have higher occurrence frequency during El Niño than during La Niña (Figure 3a). The cloud vertical distributions derived from CLay by applying the cloud optical depth threshold and only accounting for the topmost layer of the vertically separated layers are shown in Figure 3b. As only topmost cloud layers with optical depth greater than 0.3 are considered, the cloud fraction from CLay product is much smaller than those from CPro product. The cloud vertical distributions from CLay products are most relevant

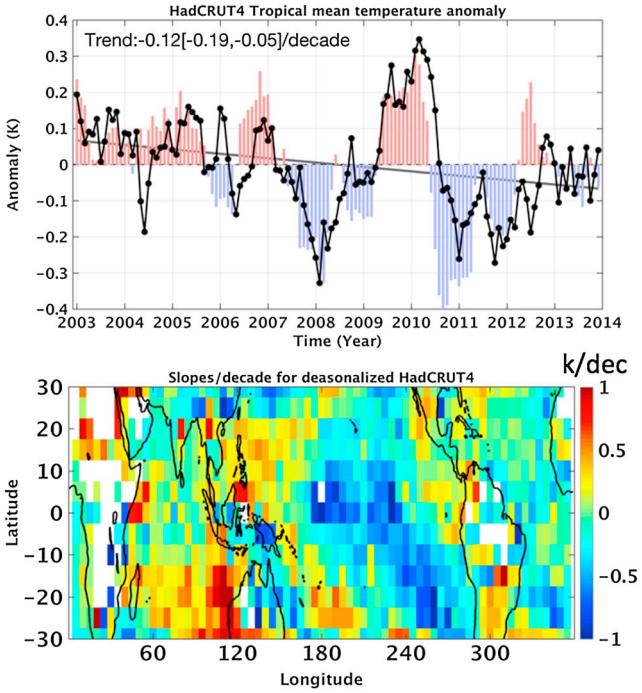

Figure 2. (a) Tropical (30°N–30°S) mean surface temperature trend (K $decade^{-1}$) derived from HadCRUT4 data and the multivariate ENSO index (scaled by 0.2). (b) Regional surface temperature trends.

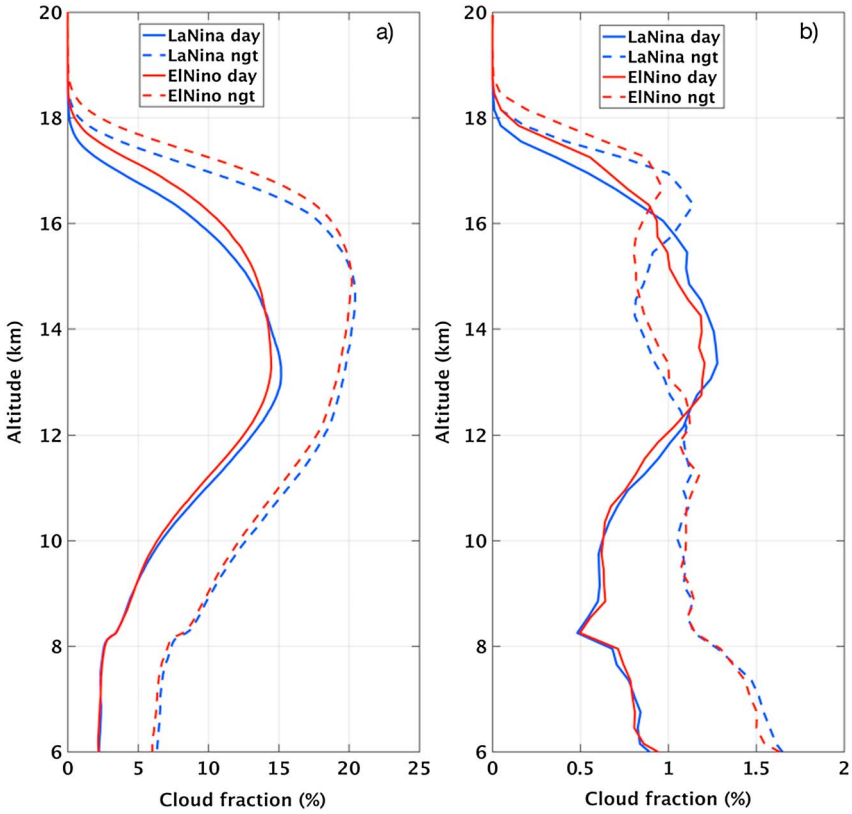

Figure 3. Vertical cloud fraction distributions over the tropics derived (a) using daytime and nighttime CALIPSO cloud profile product and (b) using cloud layer product during El Niño period (December 2009 to February 2010) and during La Niña period (December 2010 to February 2011). Red lines are for El Niño period, and blue lines are for La Niña period; solid lines are for daytime, and dashed lines are for nighttime.

to the OLR change and demonstrate how high clouds change during ENSO over the tropical regions, with higher occurrence frequency for clouds above 16 km and 17 km for daytime and nighttime during El Niño period than during La Niña period but much lower occurrence frequency for clouds right below and extended for a few kilometers. When the cloud vertical distributions are examined separately for tropical land and ocean regions, the high cloud increment during La Niña is greater over land than over ocean for both daytime and nighttime, but the peak of the nighttime profile shifts to a low altitude during La Niña over ocean whereas it remains unchanged over land (not shown).

These changes in vertical cloud distribution can explain the downward trends in daytime and nighttime OLR. However, the daytime and nighttime OLRs are changing at different rates, with the daytime trends about 30% steeper than those of the nighttime. The deseasonalized daytime and nighttime OLR difference (ΔOLR) anomaly also shows a decreasing trend significant at 95% confidence level (Figure 1c). When the ΔOLR trends are examined separately over land and ocean, all three data sets show significant trends over ocean but not over land (not shown).

Given that the CERES instruments derive the daytime OLR as the difference between the total channel and the SW channel and the nighttime OLR is simply from the total channel, it is reasonable to question whether the daytime and nighttime OLR trends are caused by the different methods used to derive them. To answer this question, we utilize the CERES WN channel and examine the daytime, nighttime, and daytime-nighttime trends using measurements on both Terra and Aqua (Figure 4). Similar to the OLR trends shown in Figure 1, both daytime and nighttime WN channel fluxes show decreasing trends that are significant at the 95% confidence level and the daytime WN flux decreases faster than that of nighttime resulting in decreasing trends in daytime-nighttime WN fluxes. These WN channel flux trends indicate that the LW flux trends are not caused by how the daytime and nighttime OLR are derived. Additionally, the regional WN flux trend distribution is very similar to that of LW flux (not shown).

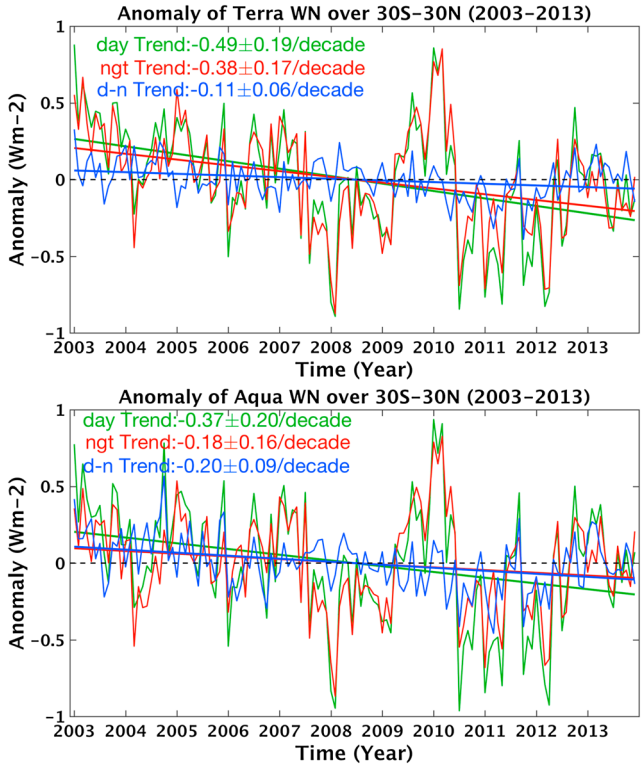

Figure 4. Deseasonalized tropical (30°N–30°S) window channel (WN in Wm^{-2}) anomalies and trends (Wm^{-2} $Decade^{-1}$) derived from CERES Terra and CERES Aqua. Daytime measurements are in green, nighttime measurements are in red, and daytime minus nighttime measurements are in blue.

Figure 5 shows the regional OLR trends calculated using monthly gridded OLR data from CERES instruments on Terra and Aqua satellites, and from AIRS instrument. Although the tropical mean OLR shows consistent downward trends for both the daytime and the nighttime observations, there are distinct regional features with statistically significant (at 95% confidence level) negative OLR trends over the tropical western Pacific (10°N–10°S, 100°E–140°E) and statistically significant positive OLR trends over the tropical central Pacific (10°N–10°S, 160°E–200°E). As the latter part of the period used in this study was dominated by La Niña events, warmer SST anomaly (Figure 2) over the western tropical Pacific caused the increasing trend in total cloud fraction (Figure 6) and the decreasing trend in total cloud effective temperature (Figure 7), which ultimately led to a downward trend in both daytime and nighttime OLR. Conversely, the colder SST anomaly over the central tropical Pacific caused the decreasing trend in total cloud fraction and the increasing trend in total cloud effective temperature and led to an upward trend in both daytime and nighttime OLR.

Are the tropical mean decreasing ΔOLR trends related to these large regional daytime and nighttime OLR trends in the Pacific? Figure 8 shows the regional ΔOLR trends calculated using data from CERES on Terra and Aqua satellites, and from AIRS instrument (white indicate that the ΔOLR trends are not statistically significant). Regions with significant ΔOLR trends are rather sporadic and are not dominated by any specific regions where large daytime and nighttime OLR trends are observed, but it is apparent that the western Pacific has more regions with negative trends than the eastern Pacific and part of the Australia is also dominated by large negative trend. When we subsample the time period used in this study by anchoring the beginning and the ending period at different ENSO phases, the daytime and nighttime OLR trends are consistent with the circulation changes associated with the ENSO events, whereas the ΔOLR trends are sporadic and we are not able to attribute the trends to any specific regions.

As illustrated in Figure 3, the cloud vertical distribution during daytime is very different from that during nighttime, and the cloud vertical distribution during El Niño is also noticeably different from that during La Niña. As the OLR is most sensitive to changes in high clouds, we investigate the trends in high cloud fraction and high cloud effective temperature to understand whether the OLR trends are caused by changes in high clouds. The CERES SYN1deg data product groups the clouds retrieved based upon MODIS observations

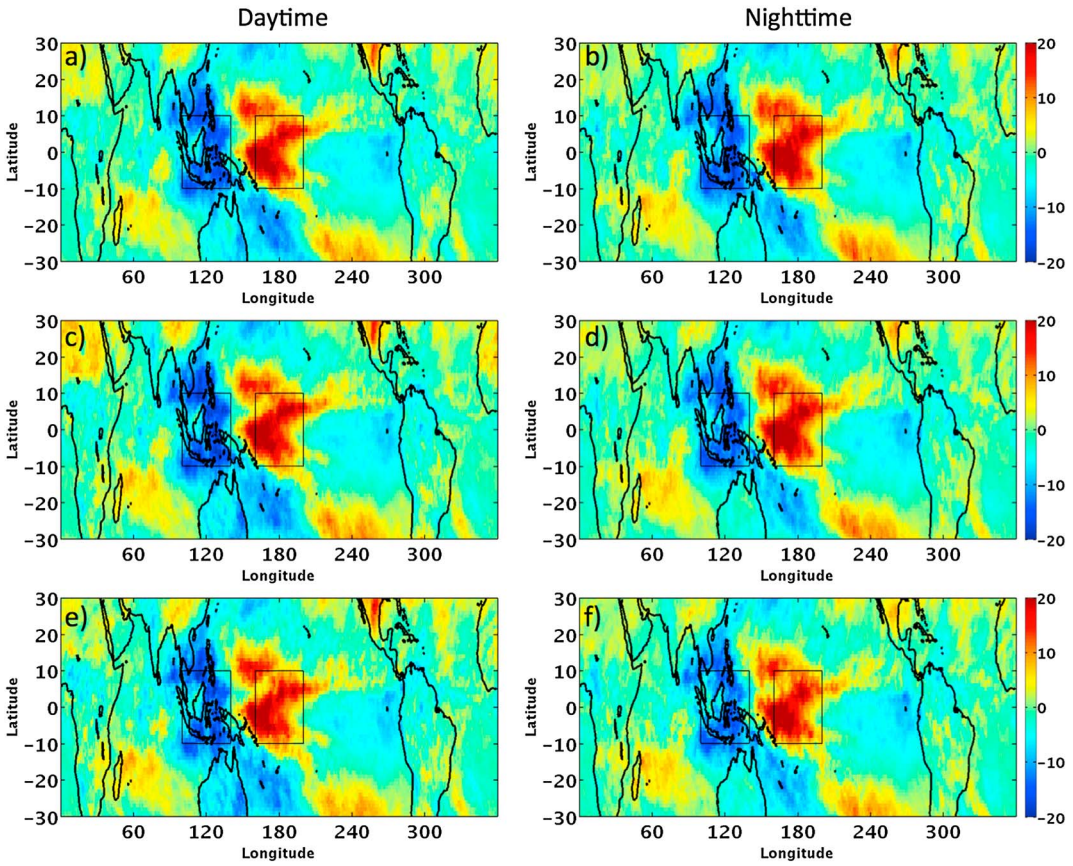

Figure 5. Regional deseasonalized OLR trends (Wm^{-2} $decade^{-1}$) derived using (a) daytime Terra OLR, (b) nighttime Terra OLR, (c) daytime Aqua OLR, (d) nighttime Aqua OLR, (e) daytime AIRS OLR, and (f) nighttime AIRS OLR. The trends are derived using data from January 2003 to December 2013.

into four layers according to the cloud effective pressure: >700 hPa, between 700 hPa and 500 hPa, between 500 hPa and 300 hPa, and <300 hPa. We define that clouds in the last two layers as high clouds. Table 3 listed the trends of high cloud fraction and high cloud effective temperature derived using daytime and nighttime MODIS observations. MODIS retrieval indicates that both daytime and nighttime high cloud fraction increased over the tropics for the period considered, and high clouds over land show a much larger upward trend than those over ocean. These upward trends in high cloud fraction can explain the downward trends in OLR for both daytime and nighttime, but do not explain why the downward trend in daytime OLR is larger than that of nighttime OLR. Rather, the tropical mean ΔOLR trend can be explained by trends in high cloud effective temperature. While the daytime high cloud effective temperature remained nearly unchanged (-0.05 ± 0.22 K per decade), the nighttime high cloud effective temperature increased slightly (0.70 ± 0.20 K per decade). This compensated for the increase in high cloud fraction, resulting in a weaker decreasing trend in OLR compared to daytime. The downward ΔOLR trend over tropical ocean can similarly be explained by the cloud property trends. However, over tropical land ΔOLR does not exhibit a statistically significant trend despite that the cloud property trends are qualitatively similar to those over the entire tropics.

The trends in MODIS high cloud fraction and effective temperature are qualitatively consistent with the cloud fraction profiles derived from CALIPSO cloud layer product for the El Niño and the La Niña cases presented in Figure 3b but less so with the CPro results (Figure 3a) possibly because different averaging method is used for the CPro data. Figure 3b shows that for both daytime and nighttime, the amount of high clouds during El Niño is less compared to during La Niña. The daytime vertical distributions of clouds during El Niño and La Niña are quite similar with a broad peak between 13 and 16 km. However, the peak cloud fraction of the nighttime clouds shifts to a lower altitude during La Niña compared to during El Niño, which partially offsets the effect on OLR of larger La Niña cloud fraction.

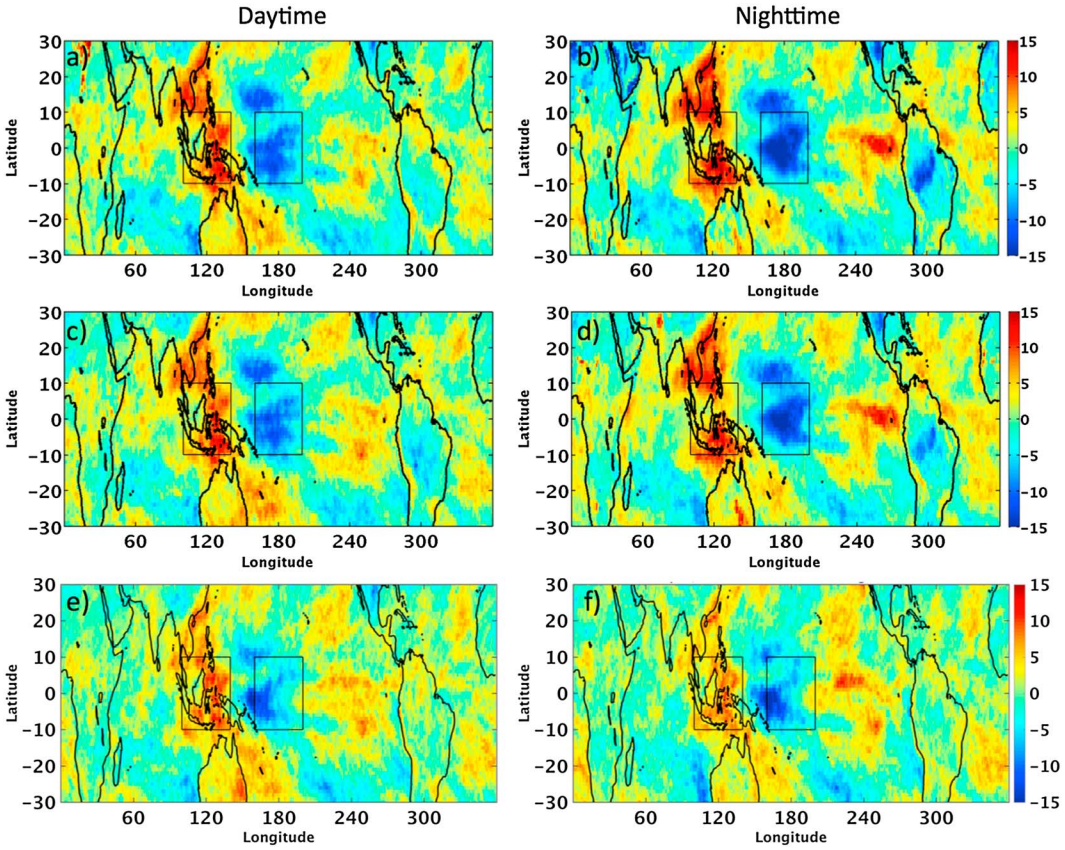

Figure 6. Regional deseasonalized cloud fraction trends (% decade^{-1}) derived using (a) daytime MODIS observations on Terra, (b) nighttime MODIS observations on Terra, (c) daytime MODIS observations on Aqua, (d) nighttime MODIS observations on Aqua, (e) daytime AIRS observations, and (f) nighttime AIRS observations. The trends are derived using data from January 2003 to December 2013.

The AIRS L3 product also reports clouds as a function of pressure level. Here we examine the changes in high clouds between 440 hPa and 10 hPa. Table 3 lists the trends of effective high cloud fraction and high cloud top temperature calculated using AIRS daytime and nighttime cloud retrievals. During this time period, only daytime cloud fraction shows an increasing trend that is significant at 95% confidence level, which is about twice the increasing trend of nighttime cloud fraction. The trends of daytime and nighttime cloud top temperature are not statistically significant.

Unlike the consistent OLR trends from CERES and AIRS, the high cloud trends derived using retrievals from MODIS and AIRS are not consistent. This is due to the different cloud retrieval methodologies used for MODIS and AIRS. The CERES cloud working group developed sophisticated cloud detection algorithms using visible and infrared channels of MODIS separately for polar and nonpolar regions and for daytime, twilight, and nighttime [*Trepte et al.*, 2010]. The daytime cloud top temperature (T_c) retrievals employed an iterative process to match the MODIS visible, infrared, and shortwave-infrared radiances with parameterizations of TOA reflectance and brightness temperature, while the nighttime T_c was determined through an iterative process that minimizes the differences between model-derived and observed values of brightness temperature differences for different infrared channels for the observed 11 μm brightness temperature [*Minnis et al.*, 2011]. The AIRS effective cloud fraction (f) and T_c are derived by comparing the AIRS observed radiances in the channels that are not affected by the solar radiation to the calculated radiances assuming the surface and atmospheric properties retrieved from AIRS are the truth and all clouds have a constant spectral emissivity of 0.9 [*Susskind et al.*, 2003]. *Kahn et al.* [2007] compared T_c and f retrieved by AIRS and MODIS team [*Platnick et al.*, 2003] by combining them into an "effective scene brightness temperature" ($T_{b,e}$), which is calculated as $fT_c + (1 - f)T_s$, where T_s is the surface temperature. They found that the $T_{b,e}$ differences between AIRS and MODIS are generally small for high opaque clouds but are much larger for low, transparent, and broken clouds. As pointed out by *Kahn et al.* [2007], the agreement in $T_{b,e}$ is a necessary, but not a sufficient, condition for

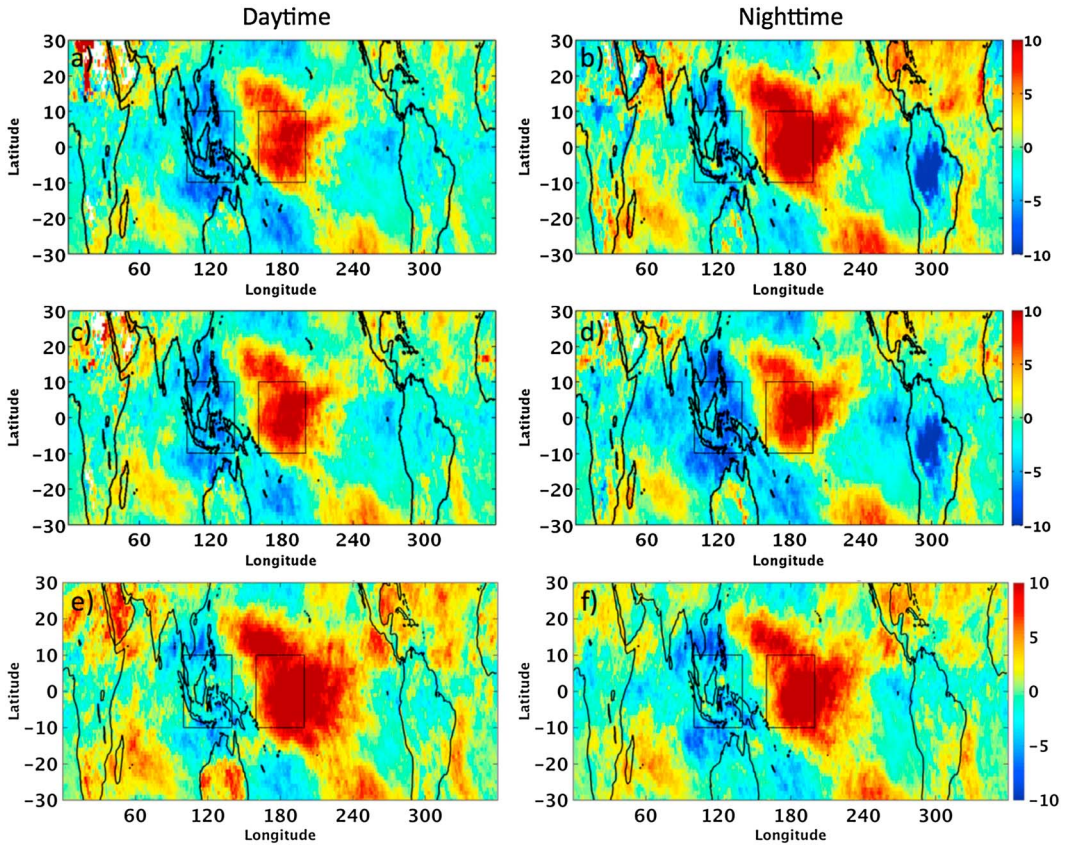

Figure 7. Regional deseasonalized cloud effective temperature trends (K decade^{-1}) derived using (a) daytime MODIS observations on Terra, (b) nighttime MODIS observations on Terra, (c) daytime MODIS observations on Aqua, (d) nighttime MODIS observations on Aqua, (e) daytime AIRS observations, and (f) nighttime AIRS observations. The trends are derived using data from January 2003 to December 2013.

individual agreement in AIRS and MODIS retrievals of f and T_c. For cases in which AIRS and MODIS $T_{b,e}$ agree, the individual fields (T_s, T_c, and f) may be different. Furthermore, they demonstrated that the spatial patterns of $T_{b,e}$ differences are systematic and not well correlated to the AIRS-MODIS radiance differences. This suggests that the inconsistencies in AIRS and MODIS cloud fields are dominated by retrieval algorithm differences rather than differences in measured radiances.

The regional trends calculated using the VIRS Tb11<235 K occurrence frequency at the Terra and Aqua overpass times show similar regional features as the cloud fraction trends in Figure 6. To understand how tropical high clouds respond to ENSO, the diurnal variations of VIRS cold cloud occurrence frequency are analyzed separately for El Niño and La Niña periods during 2003–2013. The multivariate ENSO index (MEI) [*Wolter and Timlin*, 2011] is used to determine whether a given month is in El Niño (MEI > 0.5) or La Niña (MEI<−0.5) condition. The hourly cold cloud occurrence frequencies are calculated for each calendar month for El Niño and

Table 3. Trends and 95% Confidence Intervals of High Cloud Fraction (f, %decade^{-1}) and High Cloud Effective Temperature (T, K decade^{-1}) Derived From MODIS and AIRS Observations[a]

	MODIS				AIRS			
	f (%/decade)		T (K/decade)		f (%/decade)		T (K/decade)	
	Daytime	Nighttime	Daytime	Nighttime	Daytime	Nighttime	Daytime	Nighttime
Tropical	0.44 ± 0.27	0.51 ± 0.37	−0.05 ± 0.22	0.70 ± 0.20	0.20 ± 0.17	0.09 ± 0.18	0.04 ± 0.29	−0.25 ± 0.29
Ocean	0.21 ± 0.30	0.25 ± 0.42	0.07 ± 0.24	0.83 ± 0.21	0.04 ± 0.20	−0.08 ± 0.24	−0.16 ± 0.32	−0.26 ± 0.31
Land	1.09 ± 0.65	1.22 ± 0.85	−0.39 ± 0.29	0.31 ± 0.28	0.62 ± 0.47	0.53 ± 0.57	0.29 ± 0.34	−0.21 ± 0.36

[a]Trends are derived using data from January 2003 to December 2013.

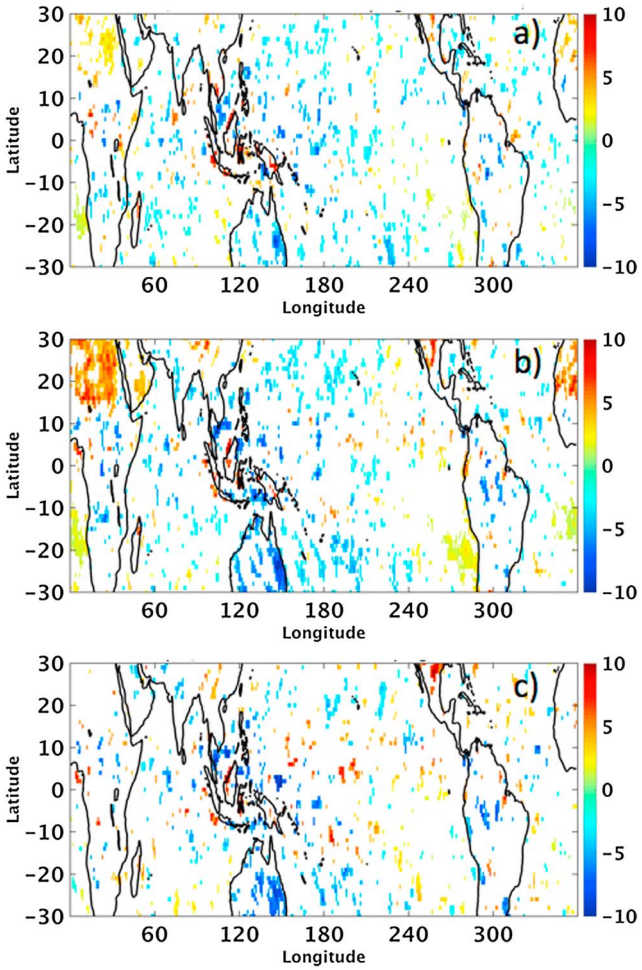

Figure 8. Regional deseasonalized ΔOLR trends (Wm^{-2} $decade^{-1}$) derived using (a) CERES Terra OLR, (b) CERES Aqua OLR, and (c) AIRS OLR. Regions shown in white indicate the trends are not statistically significant and the trends are derived using data from January 2003 to December 2013.

La Niña conditions, and these calendar months are then averaged to represent the mean diurnal variations of cold clouds during different phases of ENSO (Figure 9). The diurnal variations of clouds colder than 235 K and 210 K are much larger over land than over ocean under both El Niño and La Niña conditions. Over land, the cold cloud occurrence frequencies are larger during La Niña than during El Niño, especially at night; whereas over ocean, the cold cloud occurrence frequencies are almost identical. The larger increase during nighttime than daytime is consistent with the MODIS results but not with AIRS results shown in Table 3,

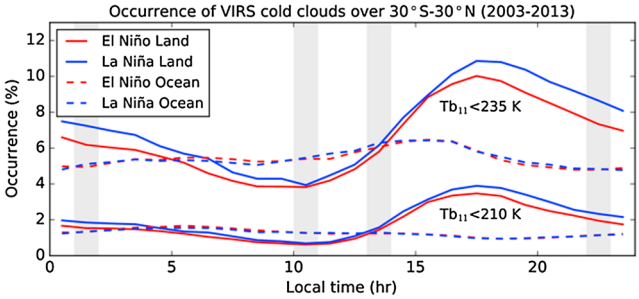

Figure 9. The diurnal variations of cold cloud occurrence frequency derived from TRMM VIRS during El Niño (MEI > 0.5) and La Niña (MEI < −0.5) conditions over land and ocean using data from January 2003 to December 2013. The cold clouds are defined by VIRS infrared brightness temperature at 10.8 μm (Tb11).

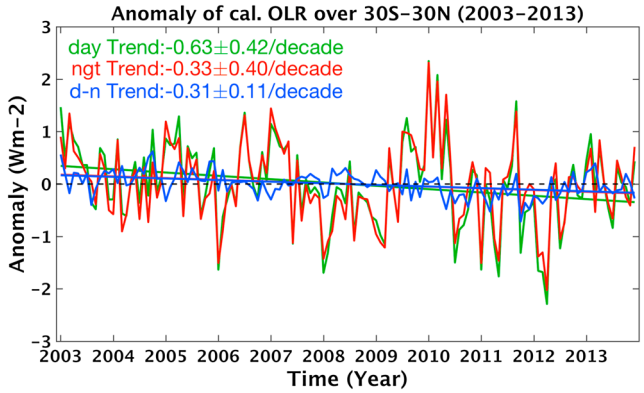

Figure 10. Deseasonalized tropical (30°N–30°S) outgoing longwave radiation (OLR, in Wm^{-2}) anomalies and trends (Wm^{-2} $decade^{-1}$) derived from the calculated OLR data in CERES SYN product.

and the larger high cloud change over land is consistent among all the data sets examined here. As the VIRS results show changes of clouds colder than 235 K (~10 km) and 210 K (~14 km) collectively, we are not able to verify whether the nighttime cloud effective temperature increases when the tropics transition from El Niño to La Niña.

The AIRS OLRs are calculated using a radiative transfer model based upon inputs from the surface, atmosphere, and cloud retrievals [*Susskind et al.*, 2011]. The CERES OLRs are based upon the radiances observed by the CERES instruments and converted to fluxes using CERES LW empirical angular distribution models [*Su et al.*, 2015]. In the CERES SYN1deg data product, both observed and computed OLRs are provided. The computed OLRs are based upon the Fu-Liou radiative transfer model with cloud properties retrieved from MODIS observation and temperature/humidity profiles from GMAO reanalysis version 5.4.1 (see details in *Rose et al.* [2013]). Figure 10 shows the tropical mean calculated OLR trends for daytime, nighttime, and their difference. Although the calculated daytime and nighttime OLR trends are smaller than those derived from CERES observations, the trends in ΔOLR are very consistent with those observed by CERES and calculated by AIRS (Table 2).

The consistent trends in OLR from observations and calculations indicate that the cloud property retrievals from AIRS and MODIS provide consistent OLR trends even though the individual cloud properties do not show consistent trends (Table 3). As noted earlier, inconsistency in cloud property retrievals is likely caused by algorithm differences. For a given set of observed radiances in the infrared, combinations of fewer clouds with lower cloud top temperature could match the observed radiances as well as the combinations of more clouds with higher cloud top temperature. Because the cloud retrieval algorithms used for MODIS and AIRS are different and the cloud retrievals have relatively large uncertainties, we are unable to pinpoint the exact cause for the larger daytime downward OLR trend than for the nighttime. However, the combined changes in cloud fraction and cloud top temperature could explain the larger decreasing trend of daytime OLR than nighttime OLR.

4. Conclusions and Discussions

Both daytime and nighttime OLR data products from CERES and AIRS show decreasing trends over the tropics using the time period from January 2003 to December 2013. The daytime and nighttime OLR trends from CERES and AIRS agree to within 0.2 Wm^{-2} per decade. These decreasing trends in OLR are caused by the ENSO variability during this time period, which started with El Niño events and ended with La Niña events. During El Niño, the tropical mean cloud fraction decreases and the cloud top temperature also decreases, but the effect of cloud fraction outweighs that of cloud top temperature, resulting in an increase in tropical mean OLR. During La Niña, the opposite occurs and the tropical mean OLR decreases. However, for the period considered (January 2003 to December 2013), the daytime and nighttime OLRs decrease at different rates, with the daytime OLR decreasing faster than the nighttime OLR. As a result, daytime-nighttime OLR exhibits a decreasing trend that is significant at the 95% confidence level, both for CERES and AIRS.

High cloud fraction and effective temperature retrievals from MODIS and AIRS were examined to understand the cause of the different decreasing rates of daytime and nighttime OLR. MODIS retrievals show that both daytime and nighttime high cloud fraction increase at approximately the same rate over the tropics for the period considered. In contrast, the MODIS high cloud effective temperature trends show distinct day and night difference. The daytime high cloud effective temperature remains nearly unchanged, whereas the nighttime high cloud effective temperature increases at the rate of 0.7 K per decade. This increase partially compensates for the increase in nighttime high cloud fraction, resulting in a smaller decreasing nighttime OLR trend compared to daytime. The MODIS cloud trends are qualitatively consistent with the changes in CALIPSO cloud vertical distribution from an El Niño event to a La Niña event. The diurnal variations of VIRS cold clouds show a larger increase of cold cloud during La Niña than during El Niño between the late afternoon and early morning, which is consistent with the larger nighttime cloud fraction increase from MODIS, but we cannot verify the MODIS cloud effective temperature change using VIRS cold cloud occurrence frequency. Cloud retrievals from AIRS show that both daytime and nighttime high cloud fractions increase, with the daytime increasing faster than nighttime, albeit at slower rates than those derived using MODIS cloud retrieval. The trends of daytime and nighttime cloud top temperature from AIRS are not statistically significant.

The inconsistent trends in cloud fraction and cloud top temperature from MODIS and AIRS are likely caused by different cloud retrieval methodologies. Multiple MODIS visible and infrared channels that are sensitive to clouds are used together to detect clouds and retrieve their optical properties, and different channel combinations are used for daytime and nighttime. The AIRS cloud retrievals only rely on the infrared channels and use the surface and atmospheric properties retrieved from AIRS as inputs.

Although the trends in cloud fraction and cloud top temperature from MODIS and AIRS are inconsistent, the OLRs computed from them are consistent. This is demonstrated by the consistent OLR trends calculated using the retrieved cloud properties. The AIRS OLRs are calculated using radiative transfer model based upon inputs from the surface, atmosphere, and cloud retrievals. CERES SYN1deg data product also include OLRs calculated using radiative transfer model with cloud properties retrieved from MODIS observations and temperature/humidity profiles from GMAO reanalysis. The decreasing trends using computed OLR from CERES SYN1deg product are smaller than those derived using CERES observed OLR for daytime and nighttime, but the daytime and nighttime difference trends are almost identical. This is also true when compared to the trends from AIRS OLR. The consistent ΔOLR trends between computed OLR from CERES SYN1deg product and AIRS OLR indicate that the retrieved daytime and nighttime cloud properties based upon MODIS and AIRS observations are radiatively consistent, despite that the individual cloud properties do not always support the decreasing ΔOLR trend.

It is apparent that the daytime and nighttime clouds respond to the SST change differently during this time period. The daytime cloud vertical distributions are not as sensitive to the SST changes as the nighttime clouds. This is presumably because that solar heating during daytime stabilizes the atmosphere and suppresses the convection over ocean and thus decouples the high cloud development with SST, whereas the lack of solar heating during nighttime makes the high cloud development more linked to the SST. However, further studies and model simulation are needed to better understand how daytime and nighttime clouds respond to SST changes.

Acknowledgments
This research was supported by the NASA CERES project. The CERES data were obtained from the NASA Langley Atmospheric Science Data Center at https://eosweb.larc.nasa.gov/project/ceres/ssf_terra-fm1_ed4a_table (ssf_aqua-fm3_ed4a_table). The CALIPSO data were obtained from the NASA Langley Atmospheric Science Data Center at https://eosweb.larc.nasa.gov/project/calipso/calipso_table. The AIRS data were obtained from the NASA Goddard Earth Science Data and Information Services Center at http://disc.sci.gsfc.nasa.gov/AIRS/data-holdings/by-data-product-V6. The VIRS data were obtained from the NASA Precipitation Processing System at https://storm.pps.eosdis.nasa.gov/storm/. The data used to produce the figures and tables in this paper are available to readers upon request. We thank Seiji Kato and Zachary Eitzen for helpful discussions, and the three reviewers for their constructive comments and suggestions which have significantly improved this paper.

References

Chen, S. S., and R. A. Houze (1997), Diurnal variation and life-cycle of deep convective systems over the tropical Pacific warm pool, *Q. J. R. Meteorol. Soc.*, *123*, 357–388.

Collins, W. D., P. J. Rasch, B. E. Eaton, B. V. Khattatov, J.-F. Lamarque, and C. S. Zender (2001), Simulating aerosols using a chemical transport model with assimilation of satellite aerosol retrievals: Methodology for INDOEX, *J. Geophys. Res.*, *106*, 7313–7336.

Doelling, D. R., N. G. Loeb, D. F. Keyes, M. L. Nordeen, D. Morstad, B. A. Wielicki, D. F. Young, and M. Sun (2013), Geostationary enhanced temporal interpolation for CERES flux products, *J. Atmos. Oceanic Technol.*, *30*, 1072–1090, doi:10.1175/JTECH-D-12-00136.1.

Fu, Q., and K.-N. Liou (1993), Parameterization of the radiative properties of cirrus clouds, *J. Atmos. Sci.*, *50*, 2008–2025.

Gray, W. M., and R. W. Jacobson (1977), Diurnal variation of deep cumulus convection, *Mon. Weather Rev.*, *105*, 1171–1188.

Gruber, A., and T. S. Chen (1988), Diurnal variation of outgoing longwave radiation, *J. Climatol.*, *8*, 1–16.

Harrison, E. F., P. Minnis, B. A. Wielicki, W. F. Staylor, G. G. Gibson, D. F. Young, and F. M. Denn (1988), First estimates of the diurnal variation of longwave radiation from the multple-satellite Earth Radiation Budget Experiment (ERBE), *Bull. Am. Meteorol. Soc.*, *69*, 1144–1151.

Hartmann, D. L., and E. E. Recker (1986), Diurnal variation of outgoing longwave radiation in the tropics, *J. Clim. Appl. Meteorol.*, *25*, 80–812.

Kahn, B., E. Fishbein, S. L. Nasiri, A. Eldering, E. J. Fetzer, M. J. Garay, and S.-Y. Lee (2007), The radiative consistency of atmospheric infrared sounder and Moderate Resolution Imaging Spectroradiometer cloud retrievals, *J. Geophys. Res.*, *112*, D09201, doi:10.1029/2006JD007486.

Kahn, B., et al. (2014), The Atmospheric Infrared Sounder version 6 cloud products, *Atmos. Chem. Phys.*, *14*, 399–426, doi:10.5194/acp-14-399-2014.
Kummerow, C., W. L. Barnes, T. Kozu, J. Shiue, and J. Simpson (1998), The Tropical Rainfall Measuring Mission (TRMM) sensor package, *J. Atmos. Oceanic Technol.*, *15*, 809–817.
Liu, C., and E. J. Zipser (2008), Diurnal cycles of precipitation, clouds, and lighting in the tropics from 9 years of TRMM observations, *Geophys. Res. Lett.*, *35*, L04819, doi:10.1029/2007GL032437.
Loeb, N. G., B. A. Wielicki, D. R. Doelling, G. L. Smith, D. F. Keyes, S. Kato, N. Manalo-Smith, and T. Wong (2009), Towards optimal closure of the Earth's top-of-atmosphere radiation budget, *J. Clim.*, *22*, 748–766, doi:10.1175/2008JCLI2637.1.
Loeb, N. G., S. Kato, W. Su, T. Wong, F. Rose, D. Doelling, and J. Norris (2012), Advances in understanding top-of-atmosphere radiation variability from satellite observations, *Surv. Geophys.*, *33*, 359–385, doi:10.1007/s10712-012-9175-1.
Loeb, N. G., N. Manalo-Smith, W. Su, M. Shankar, and S. Thomas (2016), CERES top-of-atmosphere Earth radiation budget climate data record: Accounting for in-orbit changes in instrument calibration, *Remote Sens.*, *8*, 182, doi:10.3390/rs8030182.
Lyu, C., and W. L. Barnes (2008), Ten years of TRMM/VIRs on-orbit calibrations and multiyear comparisons of VIRS and MODIS, *J. Atmos. Oceanic Technol.*, *25*, 2259–2270, doi:10.1175/2008JTECHA1110.1.
Minnis, P., et al. (2010), CERES edition 3 cloud retrievals, in *13th Conference on Atmospheric Radiation*, Am. Meteorol. Soc., Portland, Oreg.
Minnis, P., et al. (2011), CERES edition-2 cloud property retrievals using TRMM VIRS and TERRA and AQUA MODIS data, Part I: Algorithms, *IEEE Trans. Geosci. Remote Sens.*, *49*(11), 4374–4400, doi:10.1109/TGRS.2011.2144601.
Platnick, S., M. D. King, S. A. Ackerman, W. P. Menzel, B. A. Baum, J. C. Riedi, and R. A. Frey (2003), The MODIS cloud products: Algorithms and examples from Terra, *IEEE Trans. Geosci. Remote Sens.*, *41*, 459–471.
Randall, D. A., Harshvardhan, and D. A. Dazlich (1991), Diurnal variability of the hydrological cycle in a GCM, *J. Aerosol Sci.*, *48*, 40–62.
Rose, F. G., D. A. Rutan, T. P. Charlock, G. L. Smith, and S. Kato (2013), An algorithm for the constraining of radiative transfer calculations to CERES-observed broadband top-of-atmosphere irradiance, *J. Atmos. Oceanic Technol.*, *30*, 1091–1106, doi:10.1175/JTECH-D-12-00058.1.
Su, H., and J. H. Jiang (2013), Tropical clouds and circulation changes during the 2006/07 and 2009/10 El Niños, *J. Clim.*, *26*, 399–414, doi:10.1175/JCLI-D-12-00152.1.
Su, W., J. Corbett, Z. A. Eitzen, and L. Liang (2015), Next-generation angular distribution models for top-of-atmosphere radiative flux calculation from the CERES instruments: Methodology, *Atmos. Meas. Tech.*, *8*, 611–632, doi:10.5194/amt-8-611-2015.
Sui, C. H., X. Li, and K.-M Lau (1998), Radiative-convective processes in simulated diurnal variations of tropical oceanic convection, *J. Atmos. Sci.*, *55*, 2345–2357.
Susskind, J., C. D. Barnet, and J. M. Blaisdell (2003), Retrieval of atmospheric and surface parameters from AIRS/AMSU/HSB data in the presence of clouds, *IEEE Trans. Geosci. Remote Sens.*, *41*, 390–409.
Susskind, J., J. M. Blaisdell, L. Iredell, and F. Keita (2011), Improved temperature sounding and quality control methodology using AIRS/AMSU data: The AIRS science team version 5 retrieval algorithm, *IEEE Trans. Geosci. Remote Sens.*, *99*, 1–25, doi:10.1109/TGRS.2010.2070508.
Susskind, J., G. Molnar, L. Iredell, and N. G. Loeb (2012), Interannual variability of outgoing longwave radiation as observed by AIRS and CERES, *J. Geophys. Res.*, *117*, D23107, doi:10.1029/2012JD017997.
Taylor, P. C. (2012), Tropical outgoing longwave radiation and longwave cloud forcing diurnal cycles from CERES, *J. Atmos. Sci.*, 3652–3669, doi:10.1175/JAS-D-12-088.1.
Thorsen, T. J., Q. Fu, J. M. Comstock, C. Sivaraman, M. A. Vaughan, D. M. Winker, and D. D. Turner (2013), Macrophysical properties of tropical cirrus clouds from the CALIPSO satellite and from ground-based micropulse and Raman lidars, *J. Geophys. Res.*, *118*, 9209–9220, doi:10.1002/jgrd.50691.
Tian, B., B. J. Soden, and X. Wu (2004), Diurnal cycles of convection, clouds, and water vapor in the tropical upper troposphere: Satellites versus a general circulation model, *J. Geophys. Res.*, *109*, D10101, doi:10.1029/2003JD004117.
Tian, B., E. Manning, E. Fetzer, E. Olsen, S. Wong, J. Susskind, and L. Iredell (2013), *AIRS/AMSU/HSB Version 6 Level 3 Product User Guide*, Jet Propulsion Laboratory, California Institute of Technology, Pasadena, Calif.
Trenberth, K. E., J. T. Fasullo, and J. Kiehl (2009), Earth's global energy budget, *Bull. Am. Meteorol. Soc.*, *90*, 311–323, doi:10.1175/2008BAMS2634.1.
Trepte, Q. Z., P. Minnis, C. Trepte, and S. Sun-Mack (2010), Improved cloud detections in CERES Edition 3 algorithm and comparison with the CALIPSO vertical feature mask, in *13th Conference on Atmospheric Radiation*, Am. Meteorol. Soc., Portland, Oreg.
Vaughan, M. A., K. A. Powell, R. E. Kuehn, S. A. Young, D. M. Winker, C. A. Hostetler, W. H. Hunt, Z. Liu, M. J. McGill, and B. J. Getzewich (2009), Fully automated detection of cloud and aerosol layer in the CALIPSO lidar measurements, *J. Atmos. Oceanic Technol.*, *26*, 2034–2050.
Wang, H., and W. Su (2015), The ENSO effects on tropical clouds and top-of-atmosphere cloud radiative effects in CMIP5 models, *J. Geophys. Res.*, *120*, 4443–4465, doi:10.1002/2014JD022337.
Wielicki, B. A., B. R. Barkstrom, E. F. Harrison, R. B. Lee, G. L. Smith, and J. E. Cooper (1996), Clouds and the Earth's Radiant Energy System (CERES): An earth observing system experiment, *Bull. Am. Meteorol. Soc.*, *77*, 853–868.
Wolter, K., and M. S. Timlin (2011), El Niño/Southern Oscillation behaviour since 1871 as diagnosed in an extended multivariate ENSO index (MEI.ext), *Int. J. Climatol.*, *31*, 1074–1087.
Wong, T., B. A. Wielicki, R. B. Lee, G. L. Smith, K. A. Bush, and J. K. Willis (2006), Reexamination of the observed decadal variability of the Earth radiation budget using altitude-corrected ERBE/ERBS nonscanner WFOV data, *J. Clim.*, *19*, 4028–4040, doi:10.1175/JCLI3838.1.
Xu, K., and D. A. Randall (1995), Impact of interactive radiative transfer on the macroscopic behavior of cumulus ensembles. Part II: Mechanisms for cloud-radiation interactions, *J. Atmos. Sci.*, *52*(7), 800–817.
Yang, G.-Y., and L. Slingo (2001), The diurnal cycle in the tropics, *Mon. Weather Rev.*, *129*, 784–801.
Zelinka, M. D., and D. L. Hartmann (2011), The observed sensitivity of high clouds to mean surface temperature anomalies in the tropics, *J. Geophys. Res.*, *116*, D23103, doi:10.1029/2011JD016459.